Impact of local atomic stress on oxygen segregation at tilt boundaries in silicon

Yutaka Ohno,[1,a)] Kaihei Inoue,[1] Kozo Fujiwara,[1] Kentaro Kutsukake,[1] Momoko Deura,[1] Ichiro Yonenaga,[1] Naoki Ebisawa,[2] Yasuo Shimizu,[2] Koji Inoue,[2] Yasuyoshi Nagai,[2] Hideto Yoshida,[3] Seiji Takeda,[3] Shingo Tanaka,[4] and Masanori Kohyama[4]

[1]*Institute for Materials Research (IMR), Tohoku University, Katahira 2-1-1, Aoba-ku, Sendai 980-8577, Japan*
[2]*The Oarai Center, Institute for Materials Research, Tohoku University, Oarai, Ibaraki 311-1313, Japan*
[3]*The Institute of Scientific and Industrial Research (ISIR), Osaka University, 8-1 Mihogaoka, Ibaraki, Osaka 567-0047, Japan*
[4]*Department of Energy and Environment, Research Institute of Electrochemical Energy, National Institute of Advanced Industrial Science and Technology (AIST), 1-8-31 Midorigaoka, Ikeda, Osaka 563-8577, Japan*

Using the atom probe tomography, transmission electron microscopy, and *ab initio* calculations, we investigate the three-dimensional distributions of oxygen atoms segregating at the typical large-angle grain boundaries (GBs) ($\Sigma 3\{111\}$, $\Sigma 9\{221\}$, $\Sigma 9\{114\}$, $\Sigma 9\{111\}/\{115\}$, and $\Sigma 27\{552\}$) in Czochralski-grown silicon ingots. Oxygen atoms with a covalent radius that is larger than half of the silicon's radius would segregate at bond-centered positions under tensile stresses above about 2 GPa, so as to attain a more stable bonding network by reducing the local stresses. The number of oxygen atoms segregating in a unit GB area N_{GB} (in atoms/nm^2) is hypothesized to be proportional to both the number of the tensilely-stressed positions in a unit boundary area n_{bc} and the average concentration of oxygen atoms around the boundary $[O_i]$ (in at. %) with $N_{GB} \sim 50 n_{bc}[O_i]$. This indicates that the probability of oxygen atoms at the segregation positions would be, on average, fifty times larger than in bond-centered positions in defect-free regions. *Published by AIP Publishing.*
[http://dx.doi.org/10.1063/1.4975814]

A high concentration of oxygen atoms (up to 0.002 at. %) is inevitably introduced in Czochralski- (CZ-) or cast-grown silicon (Si) ingots used for photovoltaic cells. Those atoms prefer to segregate at lattice defects such as grain boundaries (GBs) during cooling ingots and cell processing, and they deteriorate the solar cell efficiencies via the formation of oxygen precipitates, that act as recombination centers[1–3] and as gettering sites for harmful metallic contaminants.[4,5] Isolated oxygen atoms would be preferable for solar cells, since the density of oxygen precipitate nuclei seems to be a crucial factor for the degradation of solar cells.[4] Precise understanding of the segregation mechanism of oxygen atoms is, therefore, one important issue to engineer the three-dimensional (3D) distribution of oxygen atoms in controlled fashions,[6] as well as to control the metallic contaminants by phosphorous diffusion gettering[7–9] and thermal[10] processes disturbed by oxygen precipitates, to produce cost-effective cells.

Impurity segregation at GBs has so far been examined microscopically using transmission electron microscopy (TEM) and atom probe tomography (APT) techniques. TEM enables us to analyze impurity configurations at heavily segregated GBs,[11–13] even though its impurity detection limit is 0.05–0.1 at. % at the best.[14] Meanwhile, APT has a detection limit that is about two orders lower than TEM, simultaneously with a spatial resolution comparable to the TEM resolution (about 0.4 nm (Ref. 15)). However, APT can analyze GB structures, such as the tilt angle and GB plane, only in special cases.[16,17] Recently, those complementary techniques are applied jointly to investigate oxygen segregation at GBs in

terms of the tilt angle.[3,17–19] Ohno *et al.* experimentally showed that the number of oxygen atoms segregating at small-angle GBs (SAGBs), composed of dislocations whose density is determined by the tilt angle, depends both on the dislocation density and on the dislocation strain.[3] Similarly, Kashammer and Sinno theoretically proposed that the number at large-angle GBs (LAGBs) is correlated with the atomic stresses localized nearby the GBs.[20] However, the microscopic correlation has not been clarified experimentally because of the difficulty of estimating local segregation that is rather sensitive to the microstructure of the GBs.[18] In this work, the 3D distribution of oxygen atoms was determined at the typical LAGBs (i.e., $\Sigma 3\{111\}$, $\Sigma 9\{221\}$, $\Sigma 9\{114\}$, $\Sigma 9\{111\}/\{115\}$, and $\Sigma 27\{552\}$ GBs which account for over 50% of all GBs in Si) using an APT technique with a high spatial resolution of 0.4 nm, and it was correlated with the atomic stresses around the GBs estimated by *ab initio* calculations based on atomic resolution scanning TEM (STEM) data. This nanoscopic finding may provide a general guidance to control compositions and band structures at GBs via oxygen segregation.

The spatial resolution in the present APT analyses was determined using a Si needle with a GB in which the $[\bar{1}\bar{1}0]$ direction of a Si grain was almost parallel to the needle axis (Fig. 1). The Si($2\bar{2}0$) lattice planes with the spacing of 0.19 nm were observed (Fig. 1(a)), indicating that the resolution parallel to the needle axis was higher than 0.19 nm. Meanwhile, the resolution perpendicular to the needle axis would be 0.4 nm,[15] approximately twice the depth resolution.[21] Therefore, the resolution normal to the GB plane, that was inclined from the needle axis, was roughly estimated to

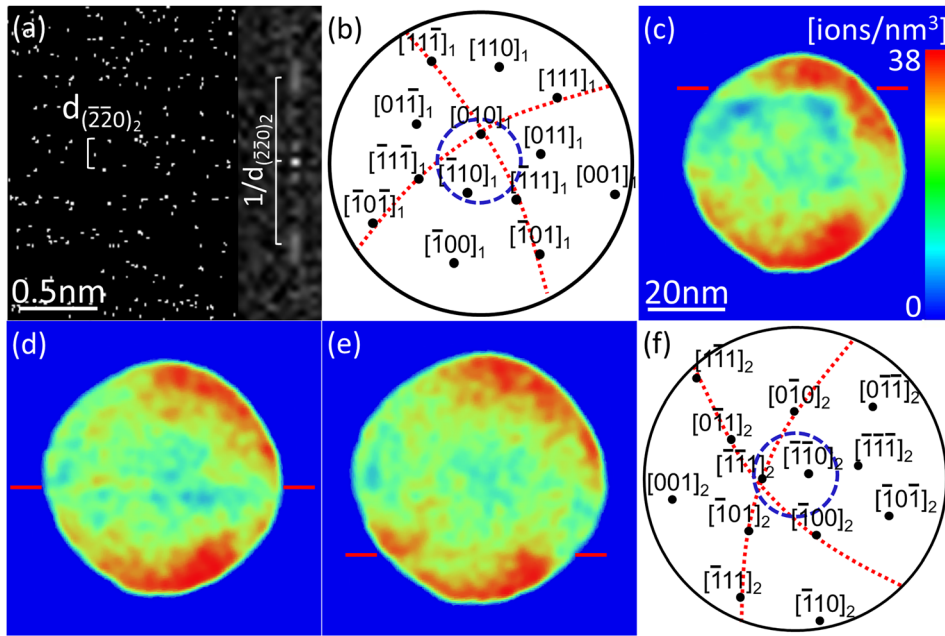a)Electronic mail: yutakaohno@imr.tohoku.ac.jp

FIG. 1. (a) Projected 3D Si map viewed nearly normal to the needle axis in the bottom grain in a Si needle with a $\Sigma 9\{114\}$ GB. The inset shows a fast Fourier transformation of the map. Stereographic projections of poles for the (b) top and (f) bottom grains. 2D Si density maps within a slice 0.2 nm thick at different depths from the apex of the needle; at (c) 300, (d) 340, and (e) 380 nm. Solid lines indicate the GB location in each figure.

be 0.4 nm. The GB location in the needle was determined with pole patterns in 2D Si density maps,[3] within slices 0.2 nm thick at different depths from the apex of the needle (Figs. 1(c)–1(e)). Since the border of the pole patterns in a 2D map was determined with a resolution of 0.4 nm, the precision of the GB position was also expected to be about 0.4 nm.

Four Si ingots were grown by the CZ method; one was doped with arsenic (As) (0.03 at. %), another was doped with boron (B) (0.04 at. %), another was co-doped with As (0.15 at. %) and B (0.08 at. %), and the other was nominally undoped. Oxygen atoms (about 0.002 at. %) were unintentionally introduced during the CZ growth. $\Sigma 3\{111\}$ GBs without GB dislocations were intentionally introduced by applying thermal shocks during growth.[17] $\Sigma 9\{221\}$, $\Sigma 9\{114\}$, $\Sigma 9\{111\}/\{115\}$, and $\Sigma 27\{552\}$ GBs were spontaneously formed as a result of the interaction of $\Sigma 3\{111\}$ GBs. Formation processes of those higher-order GBs will be discussed elsewhere.

A surface on as-grown ingots was etched with a reagent of $3HNO_3 : 1HF$, and GBs were observed on the surface. The orientation of each GB was analyzed by electron back scattered diffraction, and a $\{110\}$ foil for STEM with the GB (about 80 nm thick) was cut using a focused-ion-beam (FIB) milling under scanning electron microscopy.[17] We examined the structural property of GBs by high-angle annular dark-field (HAADF) STEM (with a JEOL JEM-ARM200F microscope), and selected pure GBs free from secondary defects such as steps and dislocations (Figs. 2(a)–2(e)), which could impact the segregation behavior.[19,22–24]

Needles for APT with a pure GB were cut nearby the location at which a foil for STEM was cut, and oxygen distributions around the GB were examined using a local electrode atom probe (Ametek, LEAP4000X HR) (Figs. 2(f)–2(j)). The concentration profile across the GB, corresponding to the integral over the width of the APT data, was
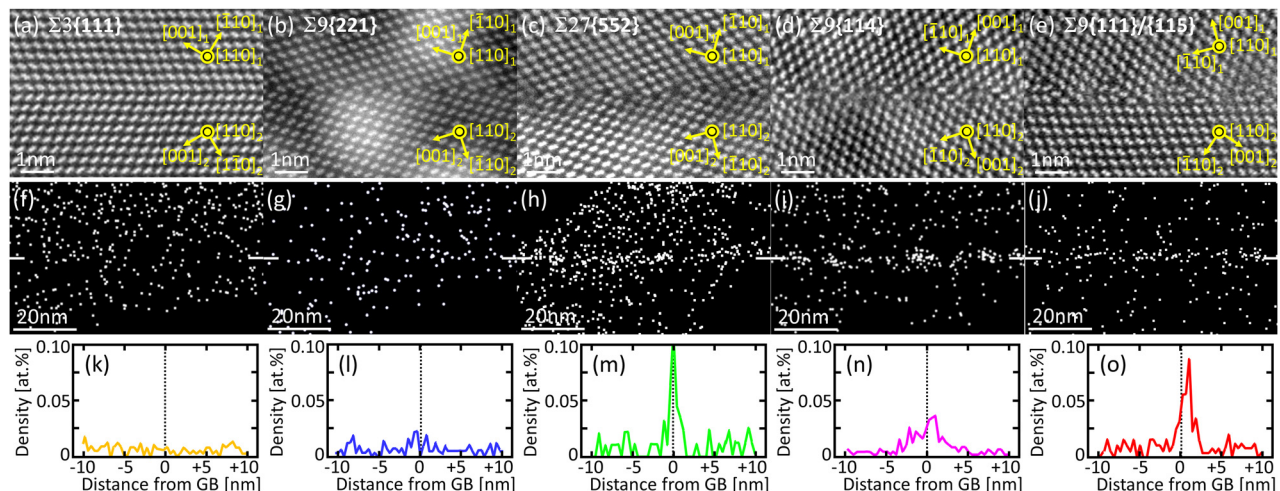

FIG. 2. (a)–(e) HAADF-STEM images of GBs viewed along the tilt axis of [110], (f)–(j) projected 3D oxygen maps viewed parallel to the GBs (in which the solid lines indicate the GB location), and (k)–(o) the concentration profile across the GBs plotted with 0.4 nm interval with an impurity detection limit of 0.005 at. %; for ((a), (f), and (k)) $\Sigma 3\{111\}$, ((b), (g), and (l)) $\Sigma 9\{221\}$, ((c), (h), and (m)) $\Sigma 27\{552\}$, ((d), (i), and (n)) $\Sigma 9\{114\}$, and ((e), (j), and (o)) $\Sigma 9\{111\}/\{115\}$ GBs.

TABLE I. GB energy E_{GB} and the number of segregating oxygen atoms N_{GB} of the typical LAGBs, and the average oxygen concentration around the GBs [O_i].

GB	E_{GB} (Jm^{-2})	N_{GB} (nm^{-2})	[O_i] (at. %)
$\Sigma3\{111\}$	$\sim$0 (Ref. [27])	$\sim$0	0.002
$\Sigma9\{221\}$	0.66 (Ref. [27])	0.013–0.020	0.002
$\Sigma27\{552\}$	0.89 (Ref. [27])	0.050–0.055	0.002
$\Sigma9\{114\}$	1.32 (Ref. [27])	0.037–0.049	0.002
$\Sigma9\{111\}/\{115\}$	>1.32 (Ref. [26])	0.039–0.060	0.002
$\Sigma5\{013\}$	0.95 (Ref. [27])	$\sim$0.006 (Ref. [19])	0.0006

determined (Figs. 2(k)–2(o)). Then, the number of oxygen atoms segregating in a unit GB area N_{GB} was estimated by the integral of the concentration profile excluded from the concentration far from the GB[25] (Table I). Oxygen atoms scarcely segregated at $\Sigma3\{111\}$ GBs, as reported,[17,28] while they segregated at the other GBs.

For $\Sigma9\{114\}$ and $\Sigma9\{111\}/\{115\}$ GBs, the oxygen concentration peaked off the GB plane in one grain by 0.4–0.8 nm (Figs. 2(n) and 2(o)). Considering the precision of the GB position (about 0.4 nm), these offsets would be significant. Therefore, the concentration profile for $\Sigma9\{114\}$ and $\Sigma9\{111\}/\{115\}$ GBs would be asymmetric with respect to the GB plane. Besides, the concentration peaked at almost equal intervals from the $\Sigma9\{221\}$ GB plane (Fig. 2(l)), and it peaked on the $\Sigma27\{552\}$ GB plane (Fig. 2(m)); the concentration profile for those GBs would be symmetric with respect to the GB plane. Similar profiles were reproduced in three different ingots, irrespective of the dopant concentrations.

Here we discuss the oxygen segregation mechanism. Since isolated oxygen impurities are not a dopant, they would not induce complicated electronic effects (extended carrier behaviors around impurity ions or drastic configurational changes of impurity atoms to localize such carriers).[27,29,30] They would adopt positions that reduce the overall lattice distortions, due to substantial differences of atomic radii of

impurities from that of Si. Hereinafter, we discuss the number of segregating oxygen atoms in terms of local atomic stresses around GBs, as proposed by Kashammer and Sinno.[20,31]

Oxygen atoms are likely to be interstitials existing at bond-centered positions in Si crystals.[32] They can induce a compressive stress,[32] since their covalent radius (0.068 nm (Ref. [33])) is larger than half of the Si radius (0.117 nm (Ref. [33])). Ohno *et al.* suggested that oxygen atoms agglomerate in the atomic sites under the tensile stress above about 2 GPa so as to compensate their compressive stresses.[3] We therefore examined the relationship of the number of segregating oxygen atoms to the local stresses at bond-centered positions in GBs using *ab initio* calculations, by which the atomistic structure of stable coincidence tilt boundaries in Si can be determined with a higher accuracy in comparison with empirical calculations, although it is difficult to discuss the effects of entropy contributions.[20]

As model GBs, we examined the symmetric $\Sigma9$ GBs with different GB planes. A cuboid cell with two $\Sigma9\{221\}$ GBs consisting of 64 atoms ($1.16 \times 2.92 \times 0.39$ nm^3) and that with two $\Sigma9\{114\}$ GBs consisting of 248 atoms ($4.09 \times 1.64 \times 0.77$ nm^3) were constructed with the STEM data, and they were relaxed by *ab initio* calculations with the projector augmented wave method based on the generalized gradient approximation implemented by the Quantum Materials Simulator (QMAS) package.[34] Stable structural models with no dangling bonds were obtained, and the [110] projection of the models reproduced the corresponding STEM images (Figs. 3(a) and 3(c)). An atomic hydrostatic stress P_{atomic} was then estimated by atomic-region integration of *ab initio* stress density obtained by QMAS code.[35,36] The fuzzy-Voronoi method[37] was used to determine the atomic regions, due to the instability of the Bader integration[36] for Si crystals. The distribution of the atomic sites under a constant stress was symmetric in $\Sigma9\{221\}$ GBs (Fig. 3(b)) while it was asymmetric in $\Sigma9\{114\}$ GBs (Fig. 3(d)), with respect to the GB plane, as a reflection of the symmetry of the bonding
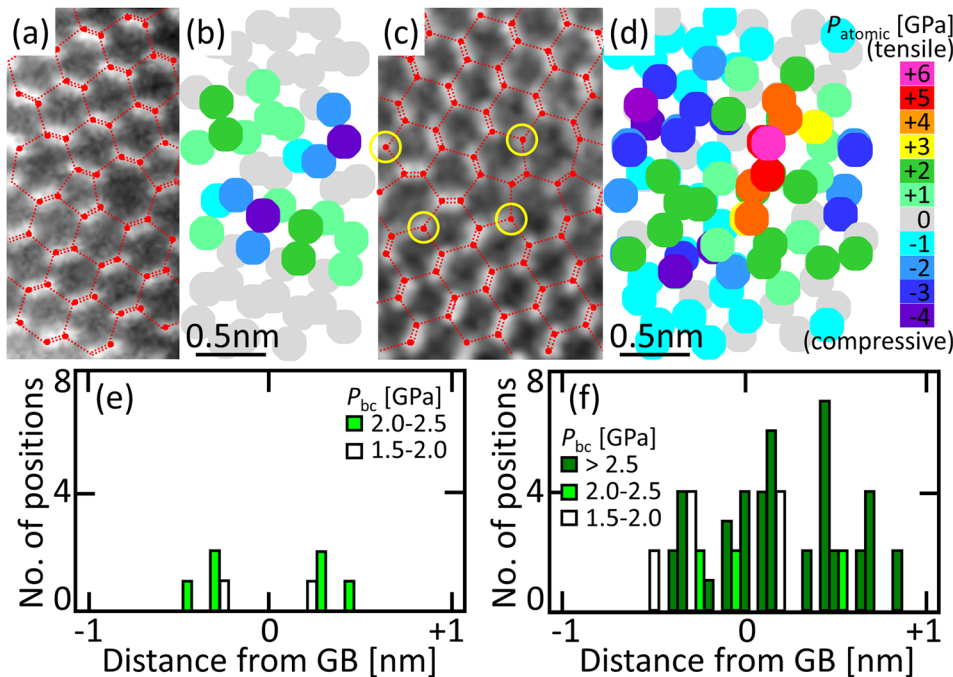

FIG. 3. ((a) and (c)) Atomic configuration and ((b) and (d)) distribution of P_{atomic} around ((a) and (b)) $\Sigma9\{221\}$ and ((c) and (d)) $\Sigma9\{114\}$ GBs. Number of bond-centered positions under a tensile stress P_{bc} above 1.5 GPa for (e) $\Sigma9\{221\}$ and (f) $\Sigma9\{114\}$ GBs.

networks in the GBs. The number of tensilely-stressed sites in Σ9{114} GBs was much larger than that in Σ9{221} GBs due to the introduction of stretched $\langle 110 \rangle$ reconstructed bonds as indicated by circles in Fig. 3(c). It is considered that $\langle 110 \rangle$ tilt GBs in Si with higher rotation angles such as Σ3{112} and Σ9{114} GBs inevitably have $\langle 110 \rangle$ reconstructed bonds in contrast to GBs with lower rotation angles such as Σ3{111} and Σ9{221} GBs without such bonds.[27]

We defined the stress at a bond-centered position P_{bc} as the average of the atomic stresses at both ends of the bond. The positions under a tensile stress in $P_{bc} \geq +1.5$ GPa or those in $P_{bc} \geq +2.0$ GPa exhibited the symmetric distribution in Σ9{221} GBs (Fig. 3(b)) while the stressed positions distributed asymmetrically in Σ9{114} GBs (Fig. 3(d)), as observed in Figs. 2(l) and 2(n). The number of the stressed positions per unit GB area n_{bc} was estimated in Σ9{221} GBs (18 nm^{-2} for $P_{bc} \geq +1.5$ GPa and 13 nm^{-2} for $P_{bc} \geq +2.0$ GPa), and the estimated number was 1/3 of the number in Σ9{114} GBs (47 nm^{-2} for $P_{bc} \geq +1.5$ GPa and 39 nm^{-2} for $P_{bc} \geq +2.0$ GPa). The estimated ratio of 1/3 agreed with the ratio of N_{GB} for Σ9{221} GBs to N_{GB} for Σ9{114} GBs, suggesting that the segregation sites would be the bond-centered positions under the tensile stresses above $1.5 \sim 2.0$ GPa. This result is consistent with the APT data for SAGBs.[3]

3D distribution of atomic stresses around GBs has previously been estimated using theoretical calculations with an empirical potential.[20] Although their accuracy is likely lower than that obtained in this work using *ab initio* methods, n_{bc} in Σ9{221} GBs estimated with the results in Ref. 20 (about 20 nm^{-2} for $P_{bc} \geq +1$ GPa and 0 nm^{-2} for $P_{bc} \geq +2$ GPa) are fairly similar to the values estimated by our *ab initio* calculations. In Σ3{111} GBs for which $N_{GB} \sim 0$ nm^{-2}, n_{bc} can be expected to be essentially zero. The empirical potential results can also be used to estimate n_{bc} in Σ27{552} GBs which is expected to be in the range of 90–30 nm^{-2}. The expected value is about 4 times larger than in Σ9{221} GBs, and this is consistent with the ratio of N_{GB} for Σ27{552} GBs to N_{GB} for Σ9{221} GBs. These results indicate that N_{GB} is in proportion to n_{bc}. However, n_{bc} in Σ5{013} GBs is expected to be larger than in Σ9{221} GBs (in the range of 40–10 nm^{-2}), though N_{GB} in Σ5{013} GBs observed in mono-cast Si is smaller than in our Σ9{221} GBs.[19] This suggests that N_{GB} is also correlated with $[O_i]$, since $[O_i]$ in mono-cast Si would be lower than in CZ-Si,[38] even though N_{GB} may depend on other factors such as the oversaturation of oxygen in the ingot and the temperature history.

The results of the present study can be summarized as measurements of N_{GB} and estimates of $n_{bc}[O_i]$ as a function of the GB energy (Fig. 4). These data suggest a strong correlation between the number of segregating oxygen atoms at GBs and the number of sites under tensile stresses above about 2 GPa with $N_{GB} \sim 50 n_{bc}[O_i]$. The proportional coefficient of 50 indicates that oxygen atoms preferentially segregate into the tensilely-stressed positions; the probability of oxygen atoms at the segregation positions would be, on average, fifty times larger than in bond-centered positions in defect-free regions. Also, in a Si ingot with a constant $[O_i]$, N_{GB} for LAGBs would be almost proportional to the GB energy E_{GB}.
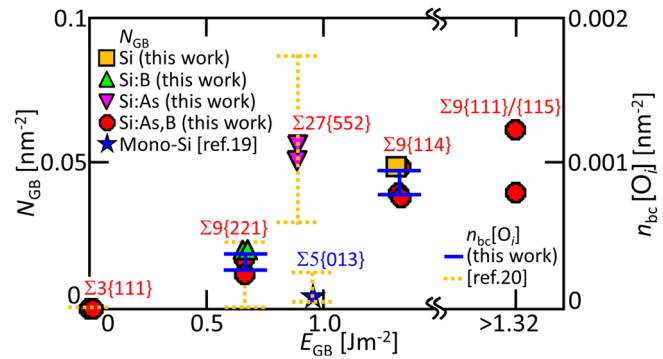

FIG. 4. Number of segregating oxygen atoms N_{GB} obtained by distinct measurements with different ingots and the number of segregation positions at GBs multiplied by the average concentration of oxygen atoms $n_{bc}[O_i]$ as a function of GB energy E_{GB}.

In summary, we have shown that isolated oxygen atoms segregate at tensilely-stressed bond-centered positions so as to reduce their atomic stresses, and that the number of segregating oxygen atoms at GBs depends on both the degree and density of atomic stresses.

[1]L. Chen, X. Yu, P. Chen, P. Wang, X. Gu, J. Lu, and D. Yang, Sol. Energy Mater. Sol. Cells **95**, 3148 (2011).

[2]J. D. Murphy, R. E. McGuire, K. Bothe, V. V. Voronkov, and R. J. Falster, Sol. Energy Mater. Sol. Cells **120**, 402 (2014).

[3]Y. Ohno, K. Inoue, K. Fujiwara, M. Deura, K. Kutsukake, I. Yonenaga, Y. Shimizu, K. Inoue, N. Ebisawa, and Y. Nagai, Appl. Phys. Lett. **106**, 251603 (2015).

[4]S. A. McHugo, H. Hieslmair, and E. R. Weber, Appl. Phys. A **64**, 127 (1997).

[5]H. Hieslmair, A. A. Istratov, S. A. McHugo, C. Flink, T. Heiser, and E. R. Weber, Appl. Phys. Lett. **72**, 1460 (1998).

[6]R. Falster and V. Voronkov, Mater. Sci. Forums **573–574**, 45–60 (2008).

[7]M. Seibt, D. Abdelbarey, V. Kveder, C. Rudolf, P. Saring, L. Stolze, and O. Vos, Mater. Sci. Eng. B **159–160**, 264 (2009).

[8]T. Sameshima, N. Miyazaki, Y. Tsuchiya, H. Hashiguchi, T. Tachibana, T. Kojima, Y. Ohshita, K. Arafune, and A. Ogura, Appl. Phys. Express **5**, 042301 (2012).

[9]D. P. Fenning, A. S. Zuschlag, M. I. Bertoni, B. Lai, G. Hahn, and T. Buonassisi, J. Appl. Phys. **113**, 214504 (2013).

[10]T. Buonassisi, A. A. Istratov, S. Peters, C. Ballif, J. Isenberg, S. Riepe, W. Warta, R. Schindler, G. Willeke, Z. Cai, B. Lai, and E. R. Weber, Appl. Phys. Lett. **87**, 121918 (2005).

[11]T. Frolov, S. V. Divinski, M. Asta, and Y. Mishin, Phys. Rev. Lett. **110**, 255502 (2013).

[12]J. F. Nie, Y. M. Zhu, J. Z. Liu, and X. Y. Fang, Science **340**, 957 (2013).

[13]Y. Ohno, K. Inoue, K. Kutsukake, M. Deura, T. Ohsawa, I. Yonenaga, H. Yoshida, S. Takeda, R. Taniguchi, H. Otubo, S. R. Nishitani, N. Ebisawa, Y. Shimizu, H. Takamizawa, K. Inoue, and Y. Nagai, Phys. Rev. B **91**, 235315 (2015).

[14]T. Walther, M. Hopkinson, N. Daneu, A. Recnik, Y. Ohno, K. Inoue, and I. Yonenaga, J. Mater. Sci. **49**, 3898 (2014).

[15]H. Akutsu, H. Itokawa, K. Nakamura, T. Iinuma, K. Suguro, H. Uchida, and M. Tada, Mater. Res. Soc. Symp. Proc. **1070**, E02-09 (2008).

[16]P. V. Liddicoat, X. Z. Liao, Y. H. Zhao, Y. T. Zhu, M. Y. Murashkin, E. J. Lavernia, R. Z. Valiev, and S. P. Ringer, Nat. Commun. **1**, 63 (2010).

[17]Y. Ohno, K. Inoue, Y. Tokumoto, K. Kutsukake, I. Yonenaga, N. Ebisawa, H. Takamizawa, Y. Shimizu, K. Inoue, Y. Nagai, H. Yoshida, and S. Takeda, Appl. Phys. Lett. **103**, 102102 (2013).

[18]M. Herbig, D. Raabe, Y. J. Li, P. Choi, S. Zaefferer, and S. Goto, Phys. Rev. Lett. **112**, 126103 (2014).

[19]Y. Ohno, K. Kutsukake, M. Deura, I. Yonenaga, Y. Shimizu, N. Ebisawa, K. Inoue, Y. Nagai, H. Yoshida, and S. Takeda, Appl. Phys. Lett. **109**, 142105 (2016).

[20]P. Kashammer and T. Sinno, J. Appl. Phys. **118**, 095301 (2015).

[21]Y. Shimizu, Y. Kawamura, M. Uematsu, M. Tomita, T. Kinno, N. Okada, M. Kato, H. Uchida, M. Takahashi, H. Ito, H. Ishikawa, Y. Ohji, H. Takamizawa, and Y. Nagai, J. Appl. Phys. **109**, 036102 (2011).

[22]T. Buonassisi, A. A. Istratov, M. D. Pickett, M. A. Marcus, T. F. Ciszec, and E. R. Weber, Appl. Phys. Lett. **89**, 042102 (2006).

[23]Y. Ohno, T. Taishi, Y. Tokumoto, and I. Yonenaga, J. Appl. Phys. **108**, 073514 (2010).

[24]G. Sarau, S. Christiansen, M. Holla, and W. Seifert, Sol. Energy Mater. Sol. Cells. **95**, 2264 (2011).

[25]The background concentration estimated with an APT concentration profile was higher than $[O_i]$, since a small amount of oxygen atoms would be occasionally introduced during FIB processes.

[26]A. Garg, W. A. T. Clark, and J. P. Hirth, Philos. Mag. A **59**, 479 (1989).

[27]M. Kohyama, Modell. Simul. Mater. Sci. Eng. **10**, R31 (2002).

[28]A. Stoffers, O. C. -Miredin, W. Seifert, S. Zaefferer, S. Riepe, and D. Raabe, Prog. Photovolt: Res. Appl. **23**, 1742 (2015).

[29]T. A. Arias and J. D. Joannopoulos, Phys. Rev. B **49**, 4525 (1994).

[30]Y. Yamamoto, K. Togase, Y. Ohno, I. Yonenaga, and S. R. Nishitani, Jpn. J. Appl. Phys. **53**, 061302 (2014).

[31]P. Kashammer and T. Sinno, J. Appl. Phys. **114**, 083505 (2013).

[32]R. Bullough and R. C. Newman, in Progress in Semiconductors, Vol. 7, edited by A. F. Gibbons and R. E. Burgers (Heywood, London, 1963), p. 100.

[33]J. A. Van Vechten and J. C. Phillips, Phys. Rev. B **2**, 2160 (1970).

[34]S. Ishibashi, T. Tamura, S. Tanaka, M. Kohyama, and K. Terakura, Phys. Rev. B **76**, 153310 (2007).

[35]Y. Shiihara, M. Kohyama, and S. Ishibashi, Phys. Rev. B **81**, 075441 (2010).

[36]H. Wang, M. Kohyama, S. Tanaka, and Y. Shiihara, J. Phys.: Condens. Matter **25**, 305006 (2013).

[37]A. D. Becke, J. Chem. Phys. **88**, 2547 (1988).

[38]K. Kutsukake, H. Ise, Y. Tokumoto, Y. Ohno, and I. Yonenaga, J. Cryst. Growth **352**, 173 (2012).